CrossMark

Homologous Microflares with Mass Ejection and Plasma Heating on the Quiet Sun

C. L. Jin[1] , G. P. Zhou[1] , and J. X. Wang[1,2]

[1] Key Laboratory of Solar Activity, National Astronomical Observatories, Chinese Academy of Science, Beijing 100101, People's Republic of China; cljin@nao.cas.cn

[2] School of Astronomy and Space Science, University of Chinese Academy of Sciences, 100049, Beijing, People's Republic of China

Abstract

Study of microflares on the quiet Sun is extremely important in learning the physics of both solar flare and atmospheric heating. Here, for the first time, we report the detailed observations of two homologous microflares from Atmospheric Imager Assembly (AIA) images and Heliospheric Magnetic Imager magnetograms in a very quiet region. The two microflares are observed clearly in the extreme ultraviolet and faintly in the ultraviolet in AIA images. They have an area of $\sim$59 Mm^2 and $\sim$46 Mm^2, and a duration of 25 minutes and 22 minutes. The magnetic cancellation continuously takes place during the microflares, and the magnetic flux decrease is apparent, with a value of $\sim$4 × 10^{18} Mx. The obvious mass ejections are observed during the microflares, and dimming occurs during and after the microflares. The velocity of mass ejection is up to 160 km s^{-1}. For the two microflares, the time of peak intensity in λ 30.4 nm precedes that of the coronal peak emission, up to 2.4–3.3 minutes. Their thermal energy is estimated to be 1.3×10^{27} erg and 2.5×10^{26} erg, respectively, which heats the corona up to 5.8 MK and 2.8 MK. There are many similarities of microflares on the quiet Sun to major flares in the active regions.

Unified Astronomy Thesaurus concepts: Solar magnetic fields (1503); Solar activity (1475); Solar ultraviolet emission (1533)

1. Introduction

Microflares, also called subflares, are small short-lived releases of stored magnetic energy in the solar atmosphere, which heat material and accelerate particles. In terms of GOES classification, they are typically B-class and A-class events, down to beyond the sensitivity limit of GOES. Energetically, they range from 10^{26} erg to 10^{29} erg, yet still demonstrate similar properties with active region flares (Hannah et al. 2011). Microflares have been observed in the Hα line (Smith & Smith 1963), soft X-ray (Schadee et al. 1983), hard X-ray (Lin et al. 1984), extreme ultraviolet (Porter et al. 1984), as well as microwave emissions (Gary & Zirin 1988). However, not all of microflares can be observed simultaneously in different wavelengths (Gary et al. 1997; Nindos et al. 1999; Qiu et al. 2004), as much depends on the heating condition of the microflares (Fang et al. 2006). Microflares are very important for understanding the process of energy release in the corona, because they ubiquitously occur in the quiet region. It is essential to trace the physical properties such as temperature and density in the course of microflares, so as to examine if their properties agree with that of the flares in the active regions.

The relationship between mass ejection from the corona, i.e., coronal mass ejection (CME), and flare has been studied in detail (Zhou et al. 2003; Vrsnak et al. 2005; Wang & Zhang 2007). However, there may be a sensitivity issue that limits the ability to study the mass ejection associated with microflares. The jets of material flowing out of the microflare region have been seen (Shibata et al. 1992; Shimojo et al. 1996; Chifor et al. 2008). Some microflares are even associated with a type III burst (Liu et al. 2004a; Christe et al. 2008). Shimizu et al. (2002) found the chromospheric ejection and the X-ray jets in some microflares. Kamio et al. (2011) observed significant coronal dimming in the surroundings of the microflare when the emission of the microflare reached its peak.

However, we still have little knowledge of the microflares, especially the microflares on the very quiet Sun. In order to understand the nature of the microflares, it is very important to study the many faces of the microflares in further detail. In particular, whether or not the microflares or nanoflares could fit in the corona with plasma and energy is a crucial issue in learning about the coronal heating and the origin of solar wind. This is the motivation for this work. In this Letter, we analyze the whole process of two microflares in a quiet region, based on the observations with the Heliospheric Magnetic Imager (HMI; Scherrer et al. 2012; Schou et al. 2012) and the Atmospheric Imager Assembly (AIA; Lemen et al. 2012) on board Solar Dynamics Observatory (Pesnell et al. 2012). We try our best to obtain fundamental properties and describe in detail the variations in a quantitative way, including the magnetic field evolution and thermodynamic atmospheric structures. The Letter is organized as follows. The observations and data analysis are described in Section 2. In Section 3 the characteristics of the microflares are studied. The discussion and conclusion are given in Section 4.

2. Observations and Data Analysis

Two microflares in the solar quiet region were observed by AIA images at about 22:58 UT on 2010 November 22 and 05:36 UT on November 23, when a couple of magnetic structures were canceling. In this study, one set of HMI line-of-sight magnetograms with a pixel size of 0$''$5 and a cadence of 45 s is selected, which covers the whole process of the two microflares. AIA images ranging from the chromosphere to the transition region and corona, with a resolution of 0$''$6 pixel size in space and 12 s cadence in time, are adopted to analyze the atmospheric structure variations during the microflares.
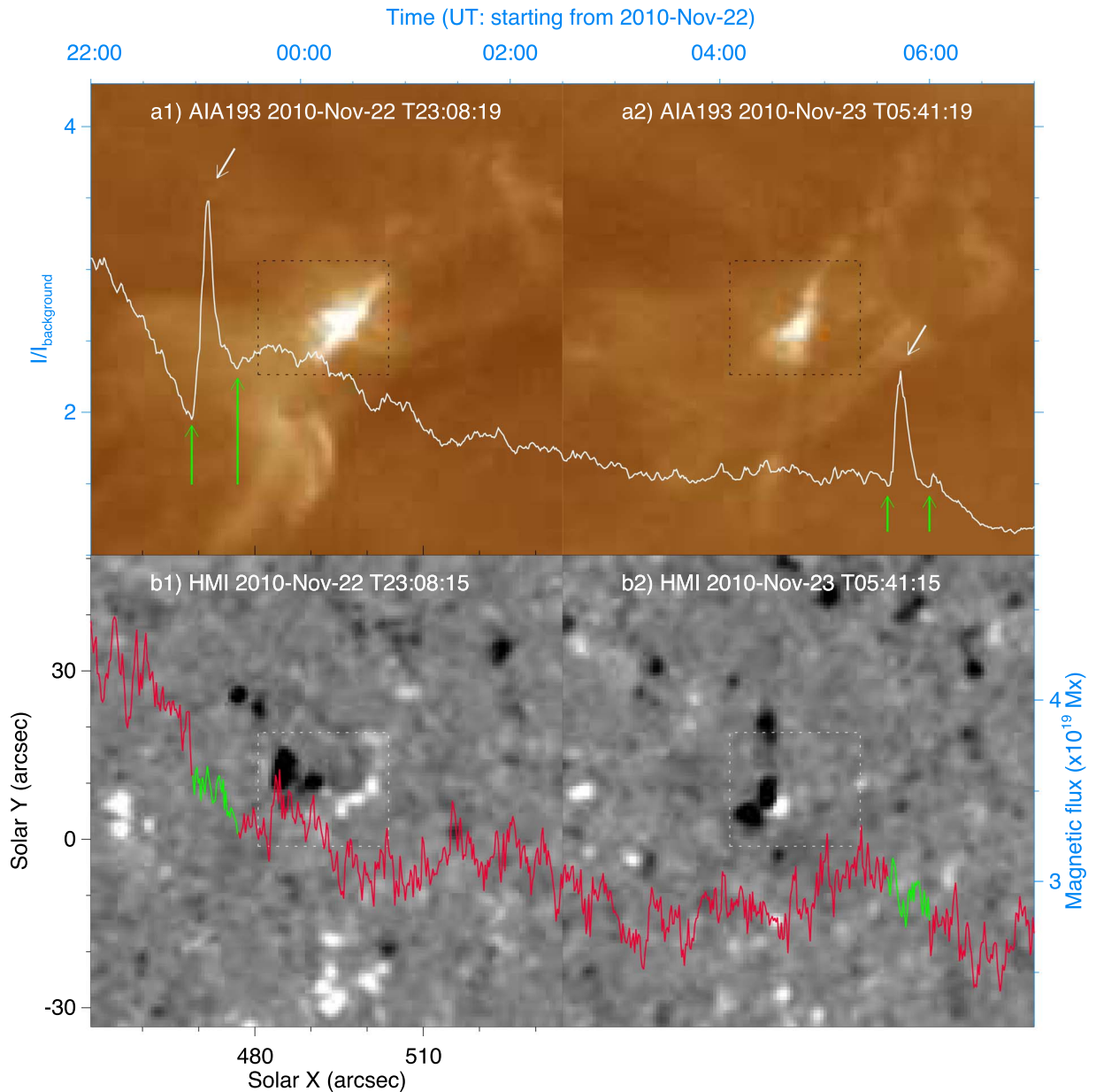
Figure 1. The images and magnetogram of the two microflares at the time of their peak intensity. The magnetic field saturates at ± 50 G. The light curve in AIA 19.3 nm and the magnetic flux change are displayed by the white and red lines, and they share a common time axis shown at the top of the figure. The regions contoured by the dotted lines are used to obtain the intensity and magnetic flux. The beginning and ending times of the two microflares are labeled by the green arrows, and for the interval of the two microflares, the curves of magnetic flux are shown by the green lines.

Following the method of estimating magnetic noise level (Hagenaar 2001; Liu et al. 2004a; Jin et al. 2011), we analyze the histogram of the magnetic field, and assume that the magnetic field has a Gaussian distribution. Finally, the distribution of the magnetic field is fitted by a Gaussian function, and the half-width of the function is defined as 1σ. In this study, the threshold of 2σ (i.e., 6 G) is adopted to extract magnetic signals.

3. The Characteristics of the Microflares

In our data set, the two microflares are observed in all wave bands of AIA images from the chromosphere to the corona. Figure 1 shows the images and magnetogram of the two microflares around the time of their peak intensity, and also displays the light curve in AIA 19.3 nm and the magnetic flux change by the white and red lines, where the light curve is normalized by the intensity in the quiet background. The two microflares are identified when the coronal intensity undergoes a sudden increase in the emission on a timescale of about half an hour, which is labeled by the white arrows in panels (a1) and (a2). From the magnetic structure evolution and the magnetic flux change shown in the bottom panel, it can be found that the two microflares take place when a couple of magnetic bipoles are continuously canceling in the quiet region. Tracing back to the couple of magnetic bipoles, it is found that the magnetic bipoles are the later decayed phase of an ephemeral region that appears in the photosphere at $\sim$02:57 UT on November 22.
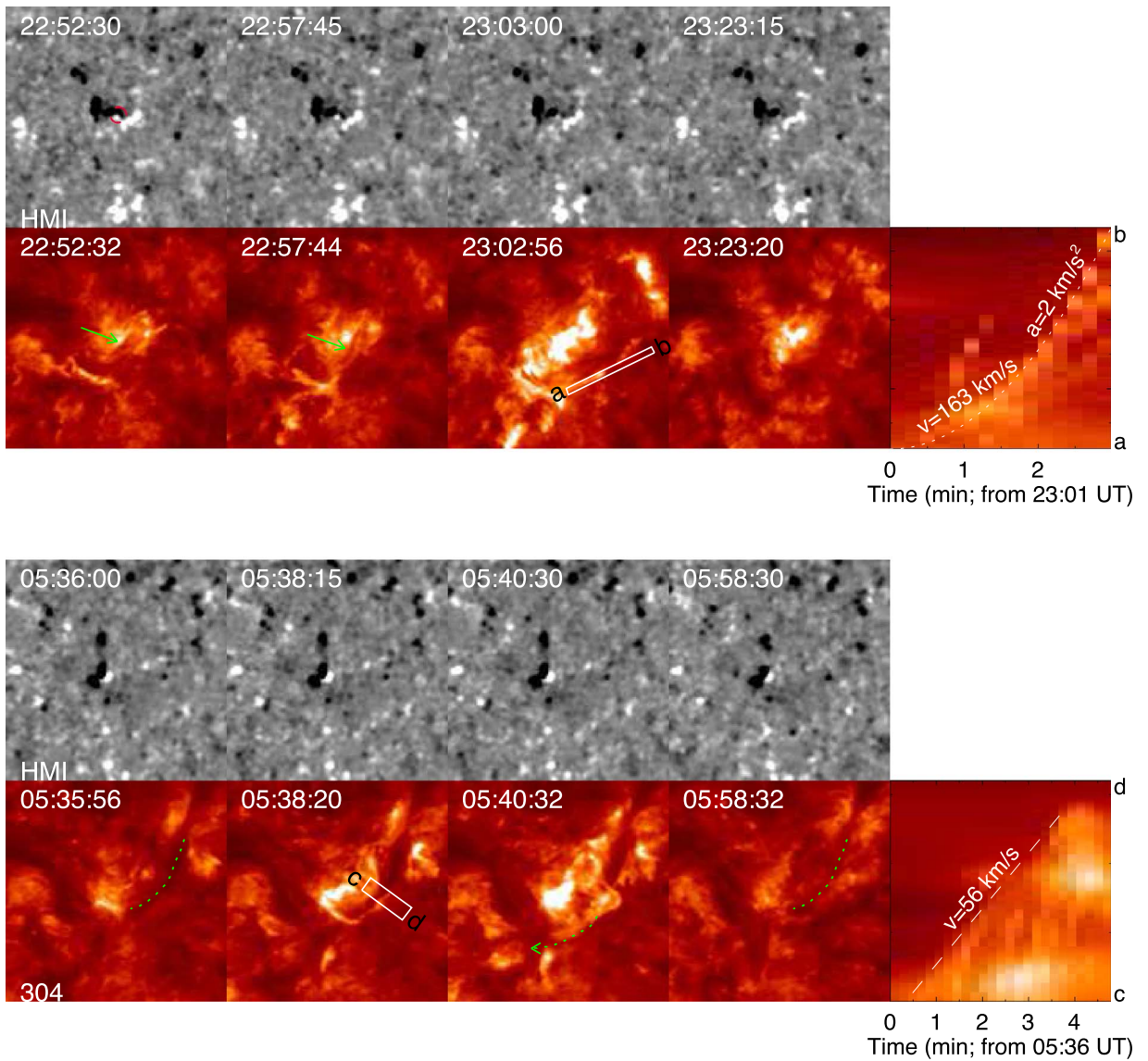
Figure 2. Top panel: the evolutions of magnetic field and image in 30.3 nm for the first microflare. The magnetic field saturates at ±30 G. The minifilament is indicated by the green arrows in the images of 30.4 nm, and the slit shown in the image at 23:02:56 UT is used to take the velocity of ejected mass. Bottom panel: the evolutions of magnetic field and image in 30.3 nm for the second microflare. A quiet minifilament is indicated by the green lines at the times of 05:35:56 UT and 05:58:32 UT. The field of view of the magnetogram and image in 30.4 nm is the same as that of Figure 1.

3.1. Magnetic Evolution and Mass Ejection during the Microflares

The top panel of Figure 2 shows a time series of magnetogram and images in λ 30.4 nm for the first microflare in the quiet region. Before the microflare, a minifilament structure is observed that spans the bright structure in the λ 30.4 nm images and is labeled by the green arrow in this figure. Then the minifilament gradually raises; after about several minutes the microflare begins. Subsequently, the minifilament is rapidly raised and ejected. In this period, some bright materials also burst out with the minifilament, with an acceleration of 2 km s^{-2}. The average velocity of mass ejection is 163 km s^{-1}, which is indicated in the lower right section of the top panel. After about 25 minutes, the microflare ends. In the peak radiance period, the spatial scale of the microflare is up to ∼19″, with an area of about 59 Mm^2. From the evolution of the magnetic field, it can be found that a couple of subbipoles cancel during the microflare, which is indicated by

the red lines in the magnetogram. The magnetic flux decreases from 3.64×10^{19} Mx to 3.26×10^{19} Mx.

After about six hours, another microflare occurs at the same location, which is shown in the bottom panel of Figure 2. Close to the position of microflare occurring, there is also a minifilament, which is labeled by the green dotted line in the images of 30.4 nm. With the radiance enhancing of the microflare, bright materials are raised with a constant speed of 56 km s^{-1}, but after 4.5 minutes the raised materials change their path and finally are ejected into the region indicated by the green dotted arrow labeled in the λ 30.4 nm images. However, the minifilament still exists after the microflare, and there is no change in position. The microflare reaches a spatial scale of about 20″ around the peak moment, with an area of approximately 46 Mm^2. Comparing the magnetic fields before and after the microflare, the magnetic cancellation continuously takes place, and the magnetic flux decreases from 3.14×10^{19}
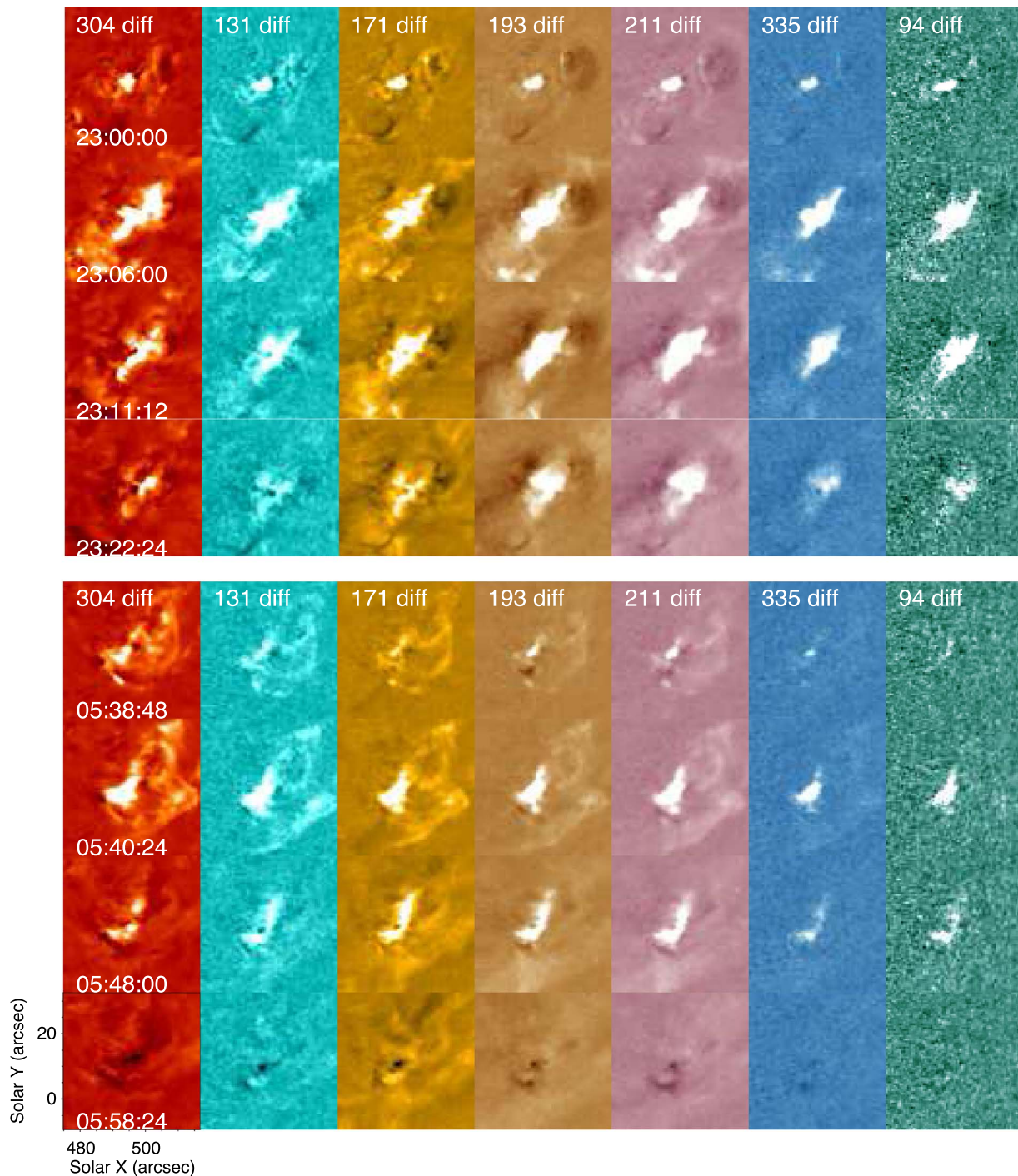
Figure 3. The variations of the atmospheric structures for the first microflare in the top panel and the second microflare in the bottom panel. The base difference images are obtained by subtracting the images at the time of 22:57:48 UT for the first microflare and 05:36:48 UT for the second microflare.

Mx to 2.74×10^{19} Mx. However, there is no observable change in the magnetogram.

3.2. Atmospheric Variation of Microflares

Base difference images in λ 30.4 nm, 13.1 nm, 17.1 nm, 19.3 nm, 21.1 nm, 33.5 nm, and 9.4 nm are derived by subtracting the images of the premicroflare to emphasize the temporal variation, which is shown in Figure 3. The top panel shows the time series of the first microflare. Enhanced emission was detected at the center of all panels. Emission of the microflare reached its peak around 23:06 UT before that

obvious dimming was observed in the microflare surrounding region in the images of λ 17.1 nm, 19.3 nm, and 21.1 nm. We analyze in detail the time series of 12 s cadence, and found that the dimming appears within a minute of the microflare start, and the dimming continues to exist after the microflare. The bottom panel of Figure 3 displays the images of the second microflare. The increased emission is detected at the center of all images at 05:38:48, 05:40:24, and 05:48:00 UT, which is similar with the first microflare. A major difference is that the dimming is observed in the microflare occurring region, and the dimming appears after the peak emission of the microflare.
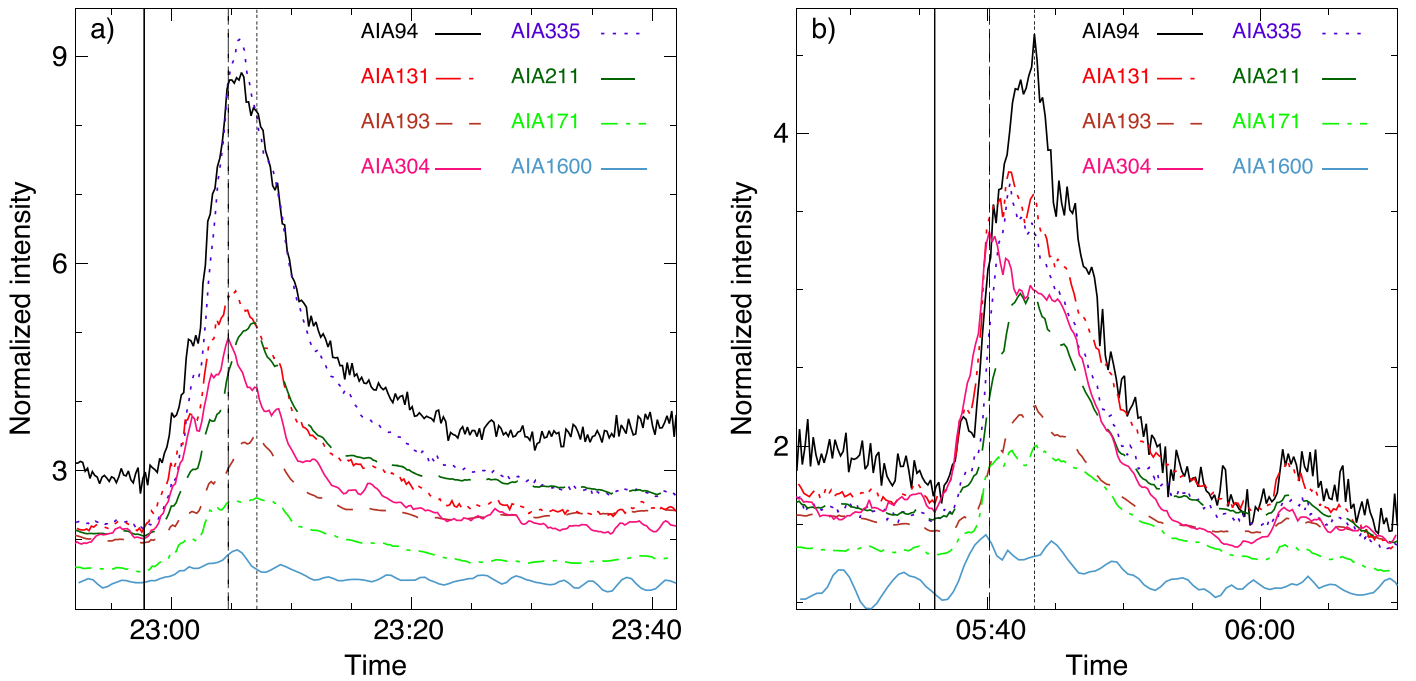
Figure 4. The light curves from the chromosphere to the corona for the first microflare in the left panel and the second microflare in the right panel, where the variation of intensity in λ 160 nm is doubled. The vertical solid lines, dashed lines, and dotted lines represent the beginning time of λ 30.4 nm enhanced emission, peak time of λ 30.4 nm enhanced emission, and latest peak time of coronal enhanced emissions.

Figure 4 displays the light curves of the two microflares, which are deduced from the region contoured by the dotted lines in Figure 1. The enhancement in the emission was observed at λ 160.0 nm for the two microflares, although it looks less obvious than other emission lines. Note that the temporal resolution of 160.0 nm is 24 s, and 12 s for other emission lines. A rapid rise in emission begins at about 22:58 UT, and flux reaches its maximum at $\sim$23:05 UT and returns the minimum at about 23:23 UT. The duration of the enhanced radiance was 25 minutes for the first microflare, which is shown in the left panel. At first glance, it is apparent that the times of the peak emissions observed in coronal lines are delayed compared with that of the peak emission in λ 30.4 nm, which is labeled by the vertical dashed line in this figure. The latest time of peak intensity is labeled by the vertical dotted line, and the delay time reaches up to 2.4 minutes. The right panel of Figure 4 shows the light curves of the second microflare. The microflare begins at $\sim$05:36 UT and ends at $\sim$05:58 UT, and the duration was 22 minutes. The microflares on the quiet Sun have a similar duration to those in the active regions (Shimizu et al. 2002), and even to large-scale flares in the active region. It is very similar to the first microflare in that the time of the peak emission in 30.4 nm precedes that of the coronal peak emission, and the time is up to 3.3 minutes.

3.3. Density and Temperature during the Microflares

The EUV intensities are converted to temperature and differential emission measure (DEM) by performing the DEM inversion method developed by Cheung et al. (2015). The EM is computed by the equation $EM_j = \int_{\log T_j}^{\log T_j + \Delta \log T_j} DEM(\log T) d \log T$, and the EM_j maps are given in the temperature range $\log T_j = [5.5, 7.5]$ with 21 temperature bins. The average temperature maps are created by

the formula $\log T_{EM} = \sum (EM_j \log T_j)/\sum EM_j$, and the total EM is obtained by the algebraic sum $EM = \sum EM_j$.

The distribution and evolution of EM and T_{EM} during the microflares are shown in Figure 5, where T_{EM} is shown by the successively blue contour lines of [2.5 MK, 3 MK, 4 MK]. EM and T_{EM} images for the first microflare are displayed in the top panel, and the obviously enhanced EM and T_{EM} during the microflare are observed, and T_{EM} is up to 5.8 MK around the peak time. In addition, the region near the microflare also shows obvious EM enhancement. However, EM and T_{EM} do not show obvious enhancement at peak time for the second microflare shown in the bottom panel, and T_{EM} only reaches 2.8 MK during the microflare. From the temperature distributions for the two microflares, it can be found that there is a peak at $\log T_{EM} = 6.3$, i.e., $T_{EM} \sim 2$ MK. This means that the plasma temperature heated by the microflares on the quiet Sun mainly concentrates on 2 MK. Compared with the microflares in active regions, the temperature of microflares on the quiet Sun is lower than that of the weakest X-ray microflare with a value of 6.7 MK (Cooper et al. 2020). The density is estimated by assuming the line-of-sight length as the width of the microflares, and it reaches 5.6×10^9 cm^{-3} for the first microflare and 2.4×10^9 cm^{-3} for the second one. The density of microflares taken by us is in the range of the microflare density in the active region, which is from 2×10^9 cm^{-3}–2×10^{10} cm^{-3} (Shimizu 1995), and even a wider range (Hannah et al. 2008).

From the temperature and density of the microflares, with the addition of their volume estimate, the instantaneous thermal energy can be calculated by the formula $E = 3 n_e k_B T V$, where k_B is the Boltzmann's constant. The microflare regions appear to be $7\rlap{.}''9$ by $18\rlap{.}''9$ for the first microflare and $5\rlap{.}''6$ by $20\rlap{.}''0$ for the second one. Assuming the region as a cylinder, this gives volumes of 3.5×10^{26} cm^3 and 1.9×10^{26} cm^3. Thus, the thermal energy is 1.3×10^{27} erg and 2.5×10^{26} erg for the two
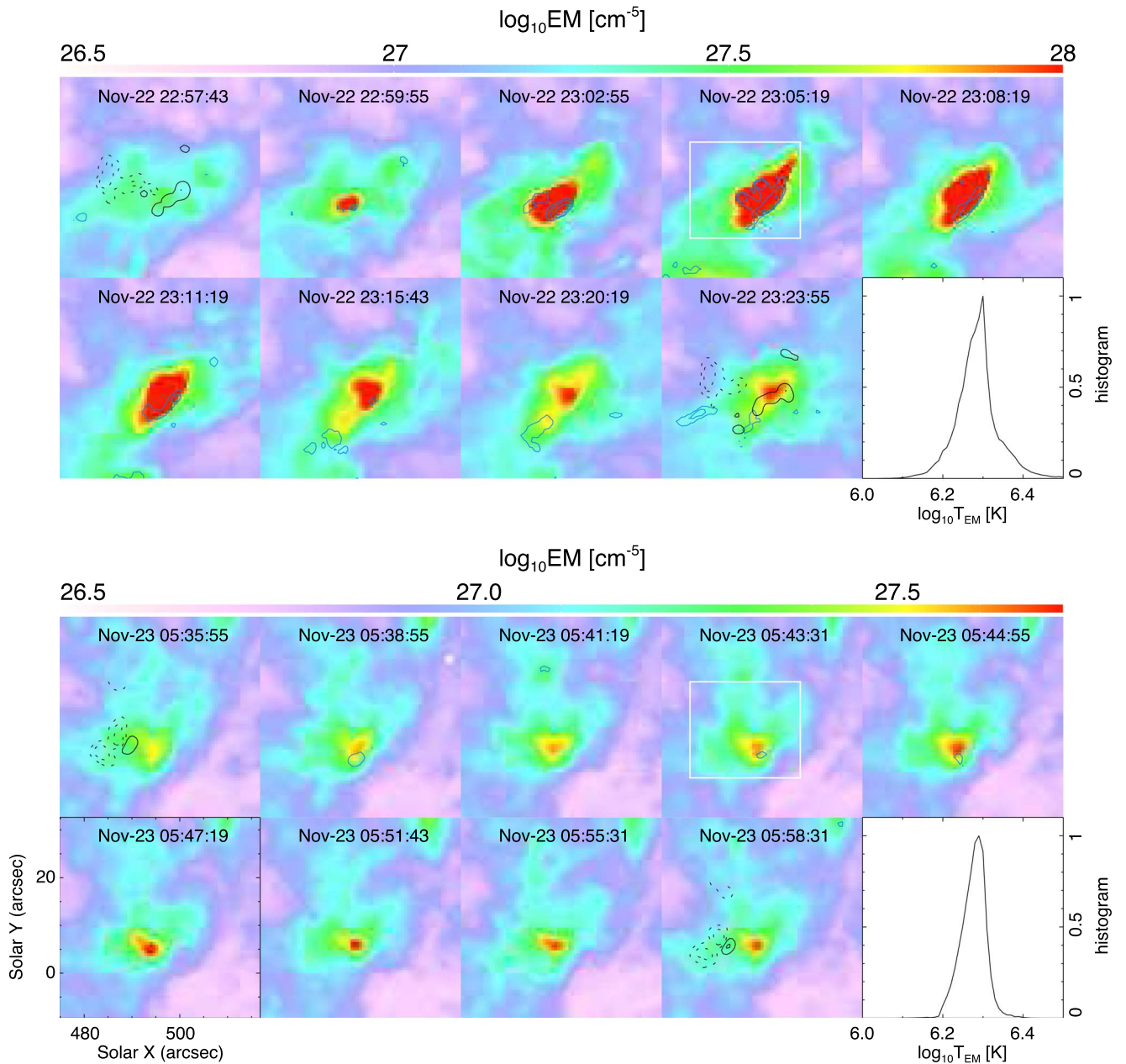
Figure 5. The evolution of EM and temperature for the first microflare in the top panel and the second microflare in the bottom panel, where the blue contour lines mean temperature values of 2.5 MK, 3 MK, and 4 MK sequentially. In the top left image and bottom right image for the two panels, the magnetic field is shown by the contour dotted lines of $[-80\text{ G}, -20\text{ G}]$ and black contour lines of $[20\text{ G}, 80\text{ G}]$. For the microflare regions contoured by the white lines, the distributions of temperature T_{EM} during the microflares are also analyzed by the histograms.

microflares, respectively. In addition, the volume estimate does not consider a filling factor in this study, making the thermal energy estimate an upper limit. Even so, the thermal energy estimated by us is lower than a typical value of 10^{28} erg taken from active region microflare statistics (Hannah et al. 2008).

4. Discussion and Conclusion

Using the AIA observations in conjunction with the HMI magnetogram, we observe two microflares during the magnetic cancellation in a solar quiet region, which shows a magnetic flux decrease with a value of about 4×10^{18} Mx during the microflares. The duration of the two microflares is 25 minutes and 22 minutes, and their spatial scale reaches up to $19''$ and

$20''$, respectively. We describe their characteristics in detail and make the main conclusions as follows:

1. We observe two typical microflares with enhanced radiance from high photosphere to the corona. The two microflares take place accompanying the mass ejection, which displays the obvious dimming during and after microflares in the corona. The velocity of the ejected mass is up to 163 km s^{-1}. As the precursor, the obviously slow rise of minifilament is observed for the first microflare.

2. From the light curve, we find that the enhanced radiance in λ 30.4 nm first reaches its peak, which precedes that of coronal peak emissions by 2.4 minutes and 3.3 minutes for the two microflares.

3. We diagnose that the plasma is heated up to 5.8 MK during the microflares in this study, and the two microflares are estimated to have a thermal energy of 1.3×10^{27} erg and 2.5×10^{26} erg, respectively.

The two microflares are driven by the magnetic cancellation on the quiet Sun, and they essentially are the same as the flares observed in the active region (Moreton & Severny 1968; Martin et al. 1985; Burtseva & Petrie 2003). The microflares on the quiet Sun share many characteristics with those in the active region, although they have relatively low density, temperature, and thermal energy (Shimizu 1995; Hannah et al. 2008). However, the behavior of the microflares in this study is very different from the schematic profile of the flare intensity at several wavelengths (Benz 2017). In the event, the energy is released in the corona, which is first seen by the lines formed in higher temperatures, and then is observed to cool down from about 10 MK through several MK, and down to the chromosphere temperature. In this study, the enhanced emission of the microflares first reaches its peak in the chromosphere, which precedes that of the coronal peak radiance by 2.4 minutes and 3.3 minutes for the two microflares, respectively. The scenario looks like the case that Hα kernel bright emissions precedes coronal soft X-ray emission in the active region flare (e.g., Kitahara & Kurokawa 1990), and the time difference between the chromosphere emission and coronal emission may be the result of the time difference between nonthermal electron beam and thermal emission as in the Neupert effect (Neupert 1968). However, the magnetic loops involved in the two homologous microflares are lower, $\sim$2–5 Mm, if estimated by the distance between the magnetic footpoints in the photosphere. Therefore, the magnetic reconnection responsible for the primary energy release must be lower that that for active region flares (Close et al. 2003). It is quite possible that major impulsive reconnection takes place in the upper chromosphere and/or transition region. Moreover, this reconnection appears to be driven by the continuous magnetic reconnection, manifested as the observed flux cancellation, in the photospheric layer with the partially ionized plasma (Wang & Shi 1993).

The two microflares are associated with the mass ejection in this study, which is similar to the relation between the flare and CMEs. Based on a statistical study, Yashiro et al. (2005) found that all the most energetic flares (>X3 level) have CMEs, and the rate for M-class flares is about 40% and for C-class about 20%. It seems to be that the smaller the flare level, the lower the CME rate. However, we know little of the CME rate of the microflares both in the active region and quiet Sun, as well as the difference of microflares without CMEs and associated with CMEs, and next we will have some statistical studies in detail.

ORCID iDs

C. L. Jin ⬤ https://orcid.org/0000-0003-4763-0854
G. P. Zhou ⬤ https://orcid.org/0000-0001-8228-565X
J. X. Wang ⬤ https://orcid.org/0000-0003-2544-9544

References

Benz, A. O. 2017, LRSP, 14, 2
Burtseva, O., & Petrie, G. 2003, SoPh, 283, 429
Cheung, M. C. M., Boerner, P., Schrijver, C. J., et al. 2015, ApJ, 807, 143
Christe, S., Krucher, S., & Lin, R. P. 2008, ApJ, 680, 149
Chifor, C., Isobe, H., Mason, H. E., et al. 2008, A&A, 491, 279
Close, R. M., Parnell, C. E., Mackay, D. H., & Priest, E. R. 2003, SoPh, 212, 251
Cooper, K., Hannah, L. G., Grefenstette, B. W., et al. 2020, ApJ, 893L, 40
Fang, C., Tang, Y. H., & Xu, Z. 2006, ChJAA, 6, 597
Gary, D. E., & Zirin, H. 1988, ApJ, 329, 991
Gary, D. E., Hartl, M. D., & Shimizu, T. 1997, ApJ, 477, 958
Hagenaar, H. J. 2001, ApJ, 555, 448
Hannah, I. G., Hudson, H. S., Battaglia, M., et al. 2011, SSRv, 159, 263
Hannah, I. G., Christe, S., Krucher, S., et al. 2008, ApJ, 677, 704
Jin, C. L., Wang, J. X., Song, Q., & Zhao, H. 2011, ApJ, 731, 37
Kamio, S., Curdt, W., Teriaca, L., & Innes, D. E. 2011, A&A, 529, 21
Kitahara, T., & Kurokawa 1990, SoPh, 125, 321
Lemen, J. R., Title, A. M., Akin, D. J., et al. 2012, SoPh, 275, 17
Lin, R. P., Schwartz, R. A., Kane, S. R., et al. 1984, ApJ, 283, 421
Liu, C., Qiu, J., Gary, D. E., et al. 2004, ApJ, 604, 442
Liu, Y., Zhao, X. P., & Hoeksema, J. T. 2004, SoPh, 219, 39
Martin, S. F., Livi, S. H. B., & Wang, J. X. 1985, AuJPh, 38, 929
Moreton, G. E., & Severny, A. B. 1968, SoPh, 3, 282
Nindos, A., Kundu, M. R., & White, S. M. 1999, ApJ, 513, 983
Neupert, W. M. 1968, ApJ, 153, 59
Pesnell, W. D., Thompson, B. J., & Chanberlin, P. C. 2012, SoPh, 275, 3
Porter, J. G., Toomre, J., & Gebbie, K. B. 1984, ApJ, 283, 879
Qiu, J., Liu, C., Gary, D. E., et al. 2004, ApJ, 612, 530
Schadee, A., de Jager, C., & Svesta, Z. 1983, SoPh, 89, 287
Scherrer, P. H., Schou, J., Bushe, R. I., et al. 2012, SoPh, 275, 207
Schou, J., Scherrer, P. H., Bushe, R. I., et al. 2012, SoPh, 275, 229
Shibata, K., Ishido, Y., Acton, L. W., et al. 1992, PASJ, 44, 173
Shimojo, M., Hashimoto, S., Shibata, K., et al. 1996, PASJ, 48, 123
Shimizu, T., Shine, R. A., Title, A. M., et al. 2002, ApJ, 574, 1074
Shimizu, T. 1995, PASJ, 47, 251
Smith, H. J., & Smith, E. V. P. 1963, Solar Flares (New York: Macmillan)
Vrsnak, B., Sudar, D., & Ruzdjak, D. 2005, A&A, 435, 1149
Wang, J. X., & Shi, Z. X. 1993, SoPh, 143, 119
Wang, Y. M., & Zhang, J. 2007, ApJ, 665, 1428
Yashiro, S., Gopalswamy, N., Skiyama, S., et al. 2005, JGRA, 110, A12
Zhou, G. P., Wang, J. X., & Cao, Z. L. 2003, A&A, 397, 1057